Available online at www.sciencedirect.com

ScienceDirect

Procedia Engineering 103 (2015) 569 – 576

Procedia Engineering

www.elsevier.com/locate/procedia

The 13th Hypervelocity Impact Symposium

High-Velocity Impact of Encased Al/PTFE Projectiles on Structural Aluminum Armor

Brett Sorensen

Army Research Laboratory, RDRL-WML-H, APG, MD 21015 USA

Abstract

In support of the U.S. Army's science and advanced technology objective in hypervelocity penetration mechanics, the Army Research Laboratory has been studying the terminal ballistics of conventional and non-conventional high-velocity kinetic energy projectiles against urban, light-armor and heavy-armor targets. The purpose is to identify and analyze both mechanisms and concepts to effectively defeat a range of targets with inert payloads using the elevated impact velocities available from future delivery systems. To this end, a series of experiments has been performed launching low-aspect-ratio aluminum and steel cylindrical projectiles, aluminum conical projectiles, and encased reactive material projectiles, with nominal masses between 200 and 240-gm, striking finite aluminum armor at nominal velocities of 2100 m/s to observe crater and spall formation and to determine the damage capacity of the debris.

Peer-review under responsibility of the Curators of the University of Missouri On behalf of the Missouri University of Science and Technology

Keywords: hypervelocity impact, KE projectiles, low density projectiles, reactive material, aluminium armor

1. Introduction

A combined experimental, computational, and analytical program was executed to examine cylindrical projectiles of nylon 6/6, 6061-T6 aluminum, and 4340 steel and 6061-T6 aluminum conical projectiles striking finite 7039 aluminum plates (50.8-mm and 76.2-mm) at nominal velocities of 2100 m/s. Additionally, Al/PTFE billets encased in aluminum, steel, and a nickel/aluminum (Ni/Al) alloy were also examined experimentally. By using several penetrator materials (and shapes) along with multiple target thicknesses, different loading functions can be applied to the target to observe potential differences in crater formation and debris character. Assuming that these constant energy impacts do result in distinct debris patterns, understanding the boundary conditions required to obtain a specific debris pattern and the ability to predict these patterns for more complex interactions would be beneficial. To this end, computational solid mechanics and analytic modeling techniques were employed to provide further insight into target response and debris formation.

Results for the solid nylon, aluminum and steel projectiles were presented in the 2007 Hypervelocity Impact Symposium.[1] This paper will present the Al/PTFE experimental results, using the nylon, aluminum, and steel cylindrical projectile data for comparison to determine if the addition of the reactive material changed the projectile/target interaction.

2. Experimental Setup

Instrumentation for these experiments included the standard striking and residual radiographs with a behind-armor-debris (BAD) collection pack. To simulate a control volume and also to completely contain the debris entering this volume, an impact chamber was constructed to simulate an interior volume behind the target. The steel impact chamber was

Peer-review under responsibility of the Curators of the University of Missouri On behalf of the Missouri University of Science and Technology
doi:10.1016/j.proeng.2015.04.074

nominally 1.37-m (4.5 ft) on a side with an interior volume of approximately 2.8-m^3 (~100 ft^3) which permitted a 1.2 x 1.2-m (4 x 4 ft) BAD pack to be placed in the back of the impact chamber with a residual x-ray cassette for the vertical plane along the right side wall. A lexan instrumentation window was placed in the left side wall to reduce x-ray absorption and to permit high-speed photography of the debris field. Pressure transducers were placed in front of the target plate, in the box behind the target plate and also in the lexan window. Finally, orthogonal striking x-rays were used to determine impact conditions. The launcher used for these experiments was a 50-mm, high-pressure powder gun capable of delivering 200 gram payloads at 2100 m/s, or about 0.5 MJ impact energy.

2.1. Projectile description

Details for the solid nylon, aluminum and steel projectiles used in the experiments are presented in Table 1 and Fig. 1. Traditional Al/PTFE experiments used Al/PTFE cylinders impacting thin bumper plates followed by a heavy anvil plate placed in an instrumented impact chamber.[2,3] The bumper plate served to fragment the material and as the fractured material impacted the anvil, reaction would occur, creating gas and pressurizing the chamber. Defeat mechanisms were perforation and then rupture from pressure of thin air-breathing structures (i.e., aircraft, missiles, etc.). Since we were interested in heavier targets, it was felt that the Al/PTFE would need a casing to assist with penetration of the target to introduce the Al/PTFE into the impact chamber. Aluminum and steel casings were selected to provide different strength casings. The nickel-aluminum casing was selected to serve as a second reactive material which would generate heat rather than gas.

The Al/PTFE billet used in the experiments was nominally 129-gm with a length of 55-mm and diameter of 36.3-mm. These dimensions were selected to yield constant projectile mass and projectile diameter for the aluminum cased projectile and the aluminum cylinder. As projectile length was fixed, the sidewall thickness for the steel casing was decreased to maintain constant mass. For all of the Al/PTFE projectiles, a 2.54-mm thick aluminum lid was used to seal the forward end of the casing and the aft end of the casings was also 2.54-mm thick. The nickel-aluminum casing was fabricated with a cold-spray process.[4] An aluminum-nickel powder mixture using a 30/70 nickel/aluminum ratio was sprayed onto a mandrel until a sufficient thickness of material existed. The mandrel and the outside of the casing were then machined to create the final part. Due to the brittleness of the material, sidewall thickness was kept the same as the aluminum casing to prevent failure at launch even though mass would increase. The lid was also pressed into place instead of using threads since the nickel-aluminum casing would not hold a thread.

Table 1. Projectile characteristics.

Material	Length (mm)	Diameter (mm)	Casing Thickness (mm)	Mass (gm)	L/Deff
Nylon	101.8	50.7	N/A	236	2.00
6061 Aluminum	51.6	43.6	N/A	217	1.18
4340 Steel	17.5	43.6	N/A	205	0.40
Al/PTFE w/ Al case	60.1	43.6	3.2	216	1.38
Al/PTFE w/ Steel case	60.1	38.1	0.44	210	1.58
Al/PTFE w/ NiAl case	60.1	43.6	3.2	231	1.38

Fig. 1. Photographs of the aluminum, steel and aluminum cased Al/PTFE projectiles.

2.2. Experimental setup

As described previously, a 2.8-m^3 steel impact chamber was constructed to simulate an interior volume and to provide a control volume. This steel structure was reinforced to withstand the impact forces and internal pressures resulting from the experiments. The aluminum target was placed on mounting studs on the front of the chamber and held in place with wedges. A lexan window was placed on the left side of the chamber to permit high-speed photography and x-ray of the behind target event. A sliding door was placed on the right side of the chamber to allow entrance and permit placement of the BAD pack and x-ray cassette. Two each dynamic and static pressure gauges were placed as illustrated in Fig. 2. The lexan window and door were wedged into place to minimize gas flow. The construction of the BAD pack used a 1/16" mild-steel plate followed by 4" of low-density fiberboard and then up to 12" of plywood. The steel plate was used to record impact signature of the debris field and the fiberboard and plywood to record velocity. By measuring the depth of penetration of each fragment, along with its mass and dimensions, an approximate velocity can be determined. Since the BAD pack used low-density fiberboard, a deluge system was configured to reduce chances of fire. After the first Ni/Al casing experiment, the fiberboard was replaced with non-flammable ceiling tiles as the deluge system proved to be insufficient.

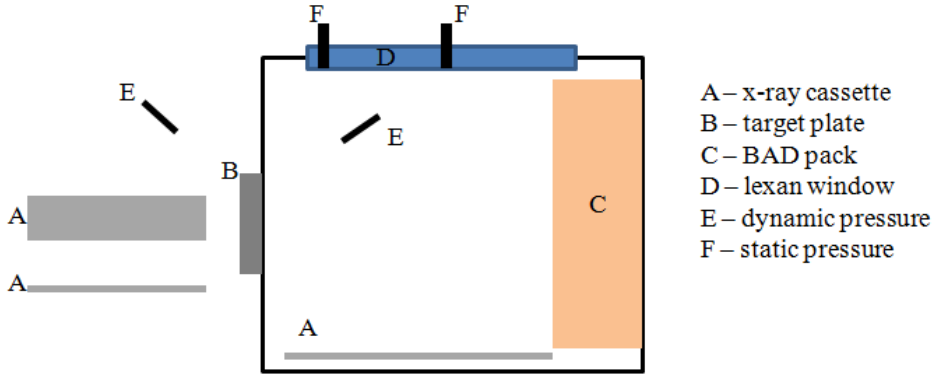

Fig. 2. Experimental setup with instrumentation and impact chamber (overhead view).

3. Results

3.1. Target response

Experimental data is presented in Table 2. For hole, exit crater and spall ring diameters, horizontal and vertical measurements were averaged and are illustrated in Fig. 3. Hole diameter (dashed white circle) was a simple definition, but exit crater diameter (black dash-dot circle) and spall ring diameter (black solid circle) were more subjective. Exit crater diameter defines the inner boundary of the spall ring and the spall ring diameter refers to the lateral size of the fully developed spall ring on the back of the target. These definitions were selected to provide consistency when comparing results. The large area represented by the shallow spall region, i.e. "scabbing", did not always form and was rarely symmetric and would skew results in later analyses. Even though the crater size measurements do not encompass the entire spall ring, these details are recovered in target mass removed and the analysis of fragment size distributions. Experiment #2501 was the first launch of the Al/PTFE with the Ni/Al casing and experienced projectile failure. Leaving the bore of the cannon, the casing split into four separate pieces and separated from the Al/PTFE billet. Since the four pieces of Ni/Al struck the face of the target, forming shallow impact craters, this data point is offered for comparison even though impact energy is not constant.

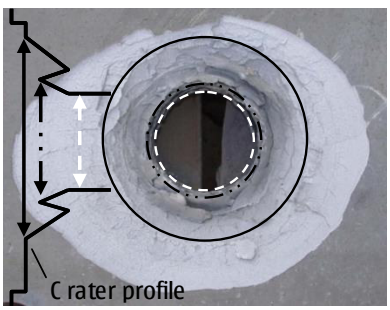

Fig. 3. Illustration of hole diameter (broken white circle), crater diameter (broken black circle), and spall ring diameter (solid black circle) measurements. Horizontal and vertical measurements are averaged for the reported value in Table 2.

Table 2. Experimental results.

	Experiment #	Projectile Type	Striking Velocity (m/s)	Total Yaw (°)	Impact Energy (MJ)	Residual Velocity (m/s)	Target Mass Loss (kg)	Hole Diameter (mm)	Exit Crater Diameter (mm)	Spall Ring Diameter (mm)
50.8mm Target	2497	Nylon	2206	6.4	0.57	661	1.99	103.0	116.0	149.0
	2498	Nylon	2261	3.9	0.60	815	1.99	104.5	116.5	156.5
	2495	Alum	~2145*	ND	~0.50	1250**	1.61	87.0	94.0	156.5
	2815	Alum	2137	1.44	0.48	1011	1.81	98.0	106.5	147.5
	2813	Steel-30	2135	1.38	0.47	1179	1.81	79.5	91.0	138.5
	2818	Steel-30	2144	3.47	0.47	1178	1.90	76.0	88.0	141.0
	2501	Al/PTFE	2115	5.5	0.29	1004	1.41	78.1	90.1	144.6
	2500	Al/PTFE-Al	2115	0.0	0.48	1167	1.81	96.8	123.2	156.8
	2499	Al/PTFE-St	2163	4.5	0.49	1156	1.54	88.1	104.1	153.2
	2506	Al/PTFE-NiAl	2161	1.6	0.54	1115	1.68	90.4	106.1	163.8
76.2mm Target	2496	Alum	~2140*	ND	~0.50	592	3.17	82.1	117.5	163.5
	2816	Alum	2113	1.51	0.47	606	3.08	78.5	83.0	184.0
	2814	Steel-30	2085	6.26	0.45	585	3.54	87.0	100.5	174.0
	2817	Steel-30	2132	2.3	0.46	711	3.54	76.5	99.0	174.0
	2504	Al/PTFE-Al	2211	5.3	0.53	697	3.13	82.3	94.3	216.8
	2503	Al/PTFE-St	~2135*	N/D	0.48	684	2.81	78.6	87.4	192.9
	2505	Al/PTFE-NiAl	2128	2.6	0.53	624	3.18	77.5	99.5	219.9

* - Striking x-rays lost. Velocity estimated from gun pressure data
** - Residual x-rays lost, velocities estimated from video, +/- 80 m/s error

The target mass loss and crater diameter results from Table 2 are plotted in Fig. 4. Here, the results from the aluminum projectile vs. 50.9-mm plate are used as a baseline to normalize the target mass removed and diameter results. Starting with hole diameter, there is little to comment on other than that for the 76.2-mm target, the holes are slightly smaller than for the 50.8-mm target and very consistent. However, for spall ring diameter, the following observations can be made: the 50.8-mm spall rings are very consistent; the 76.2-mm spall rings are larger than the 50.8-mm spall rings; and for the 76.2-mm spall rings, the Al/PTFE projectiles had larger spall rings than the inert aluminum and steel projectiles. With exception of the aluminum projectile, the spall rings for the 76.2-mm target were 25 – 35% larger for each projectile when compared to the respective result in the 50.8-mm target. For the aluminum projectile, the increase was only 15%. As noted in our first paper, a larger spall surface should be seen in the 76.2-mm target since the spherical shock wave can expand to a larger lateral area before the magnitude of the reflected wave falls below the spall threshold.

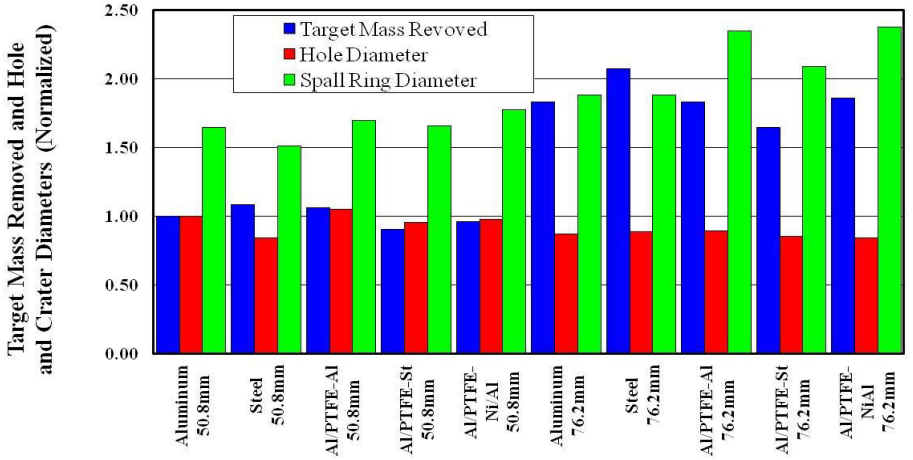

Fig. 4. Target mass removed, hole diameter, and spall ring diameter normalized by the aluminium 50-mm results.

To examine mass loss in more detail, Fig. 5 plots mass loss normalized by impact energy and includes the Al/PTFE billet only data point. Ignoring Al/PTFE only data point for the moment, Fig. 5 shows that after normalizing for impact energy aluminum and steel projectiles remove more mass than the cased Al/PTFE projectiles; on average, 10% for the 50.8-mm target and 20% for the 76.2-mm target. But clearly, the steel projectile in the 76.2-mm target appears to be different. Examining the 76.2-mm data, the aluminum projectiles remove 10% more material than the cased Al/PTFE projectiles while the steel projectile removes 25% more material than the cased Al/PTFE projectiles and 15% more material than the aluminum projectiles. However, examining only the aluminum and steel data, the steel projectile removes 13% more target material in the 50.8-mm target than the aluminum projectile and 20% in the 76.2-mm targets; much smaller differences. A possible explanation lies in the projectile / target geometries. Since the steel projectile is only 33% of the length of the aluminum projectile, there is time for the reflected wave in the penetrator to reach the penetration front before the spherical shock reaches the rear surface of the target, thus increasing the pressure slightly at the penetrator / target interface. Comparing the cased Al/PTFE projectiles to the aluminum projectiles, the Al/PTFE projectiles remove 96% and 90% of the mass that the aluminum projectiles. Even though the lengths are similar, the sound speed in the aluminum is at least twice that of Al/PTFE, so the length scale trend is consistent. Projectile strength trends are the same as length, however, with impact velocity above 2100 m/s, projectile strength should not be an issue.

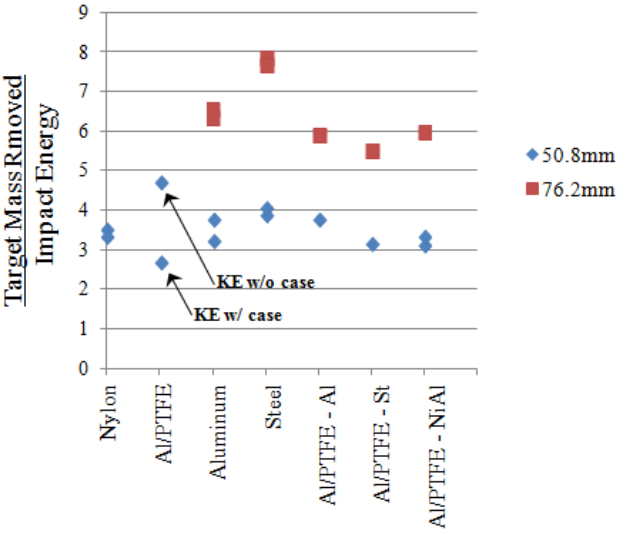

Fig. 5. Plot of target mass removed normalized by impact energy where mass is in kg and energy in MJ.

Returning to the Al/PTFE only data point, this data point is computed using impact energies with and without the case mass to bracket the actual value. While the casing material did impact the target surface, only shallow craters resulted and it is assumed that the mass loss is small and that the majority of mass removed was from the Al/PTFE impact. Thus, using KE for the Al/PTFE only, normalized mass loss is 20% higher than the steel data point, which seems unreasonable. If an average value between without case KE and with case KE is used, this result would be similar to the other Al/PTFE data points. Regardless, looking back to Table 2, the target mass loss without normalizing for impact energy shows that the Al/PTFE projectile removed only 75 – 80% of the mass as compared to the aluminum and steel projectiles, which would be undesirable to create damage behind the target.

Finally, a comment on the nylon data point. On the surface, mass loss efficiency appears to be similar to the other projectiles. However, since the diameter of the nylon projectile is 10% larger, if mass loss is further normalized by the ratio of projectile areas (A_{Al}/A_{Nylon}), mass loss is now 20% less than the Al projectile. This continues the trend that mass loss is attenuated by the increased time for the reflected wave in the projectile to reach the penetration interface.

3.2. Fragment response

Figure 6 presents photographs of the rear target surface, the front of the mild-steel witness plate and the residual x-rays. The first observation is the presence of soot on the target plates of the Al/PTFE projectiles and the scorch marks on the steel witness panels of the 50.8-mm targets. Review of the high-speed photography also indicates that there was much more combustion for the Al/PTFE projectiles against the 50.8-mm plate, which will be discussed later. The second observation is that the 50.8-mm witness plates have more impacts and smaller holes. This is also obvious when examining the residual x-rays, where the debris particles are smaller exiting the 50.8-mm target. This is consistent with Grady [5] since the 50.8-mm targets result in higher residual velocities and thus, higher strain rates, producing smaller fragments. Other observations are that only the Al and steel projectiles vs. the 50.8-mm target produce an expanding ellipsoidal debris cloud. All other projectile/target configurations yield a more chaotic debris cloud. This may be due to the timing of the x-ray flashes, or 1) being closer to the limit velocity, 2) lower impedance and/or early energy release from the Al/PTFE affecting debris character. Finally, only the Al and steel projectiles produce scabbing on the back surface of the targets.

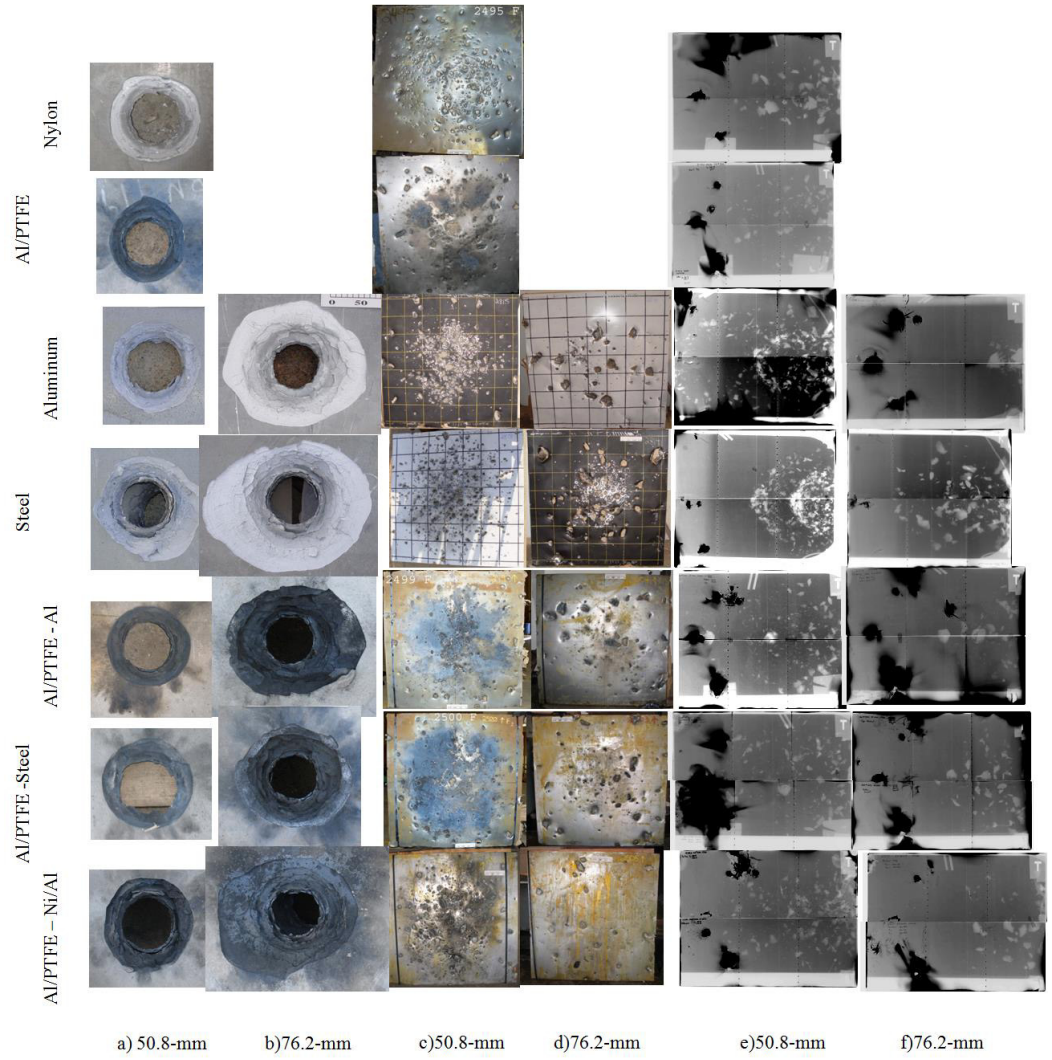

Fig. 6. Photographs of the target rear faces, the mild-steel plate in the BAD pack and the residual x-rays.

To examine fragment mass distribution in more detail, all fragments from the BAD pack and from inside the impact chamber were collected and measured. From the 50.8-mm targets, an average of 42% of the lost target mass was collected ranging from a low of 32% and a high of 55%. For the 76.2-mm target, the average was 51% with a low of 39% and a high of 65%. After measuring each fragment, masses were sorted and binned with the results plotted in Fig. 7. Here, Fig. 7a plots the percentage of the total mass sorted into each of the six bins listed in the legend on the right. For the aluminum and steel projectiles, averages of two experiments are used, where single experiment results exist for the Al/PTFE experiments. The primary observation in Fig. 7a is the dramatic increase in the heaviest bin (M > 50 gm) for the 76.2-mm target. Figure 7b plots the percentage of the number of fragments in each bin and again, the number of fragments in the heaviest bin is substantially higher for the 76.2-mm target. This increase in the number of fragments over 50gm explains how mass distribution moved so much in the thicker target plate. However, the combined percentage of fragments in the two lightest bins is not that different between the plates. If one were to assume that the small fragments originate near the center of impact and the heavy fragments from the outer portion of the spall ring, an explanation can be arrived at. Repeating this analysis using only the fragments recovered from the BAD pack, thus eliminating low velocity particles with larger departure angles, resulted in many fewer fragments, but with the same mass and number distributions. Since the residual velocity for the 76.2-mm targets is half that of the 50.8-mm targets, the different strain-rates at target failure are responsible for the difference in fragment size distributions.

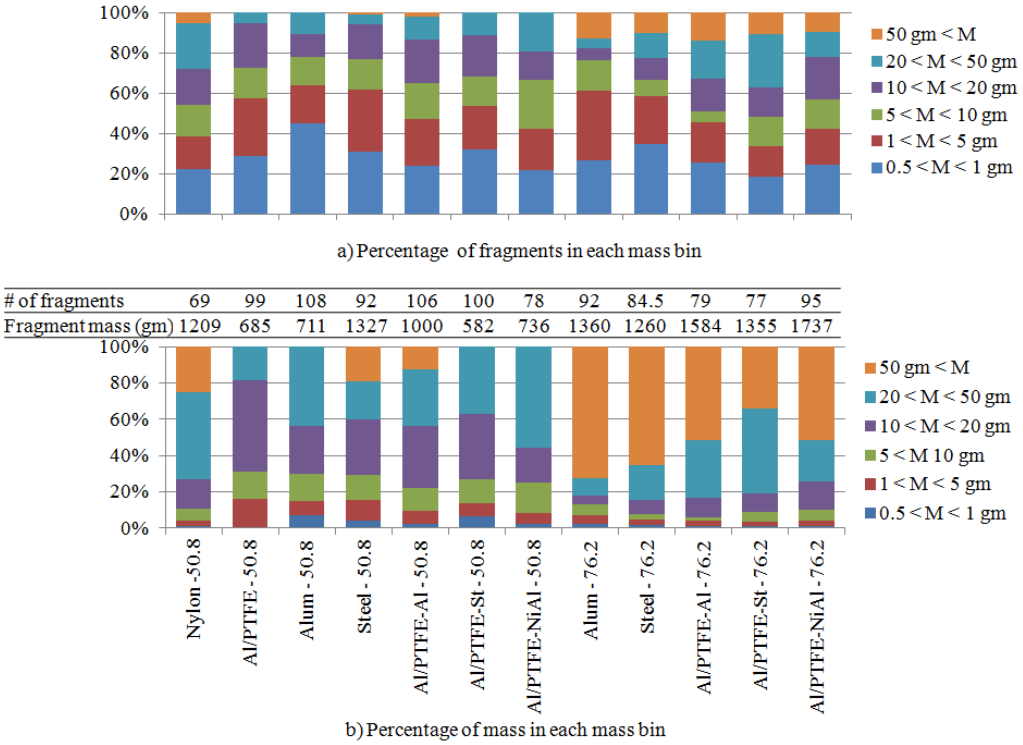

Fig. 7. Fragment count and fragment mass distributions.

3.3. Al/PTFE combustion

The high-speed photography showed that in all cases with the Al/PTFE fill, there is a large expanding fireball upon target failure. Figures 8 and 9 provide select images from 50.8 and 76.2-mm targets, respectively. In Fig. 8, frames A – C show the expanding fireball with debris exiting the fireball at frame C and impacting the steel witness plate in frames D and E. In frames F – H, combustion of the Al/PTFE is seen with a second fireball starting on the front of the BAD pack and moving forward in the impact chamber. In frame K, secondary combustion begins and initially moves toward the front of the chamber and as seen in frame N, moves back to the center of the chamber. In frame O, flame and smoke from the front of the impact chamber can be seen flowing around the side of the chamber. In Fig. 9, debris can be seen exiting the fireball in frames C – D and impacting the steel witness plate in frame E. There is a small amount of combustion which quenches very rapidly. Unlike in Fig. 8, the fireball created at target failure expands to a point just short of the steel witness plate and stops. There is a small amount of secondary combustion at the leading edge of the fireball, but it is not as large, does not last as long, and is stagnant. It is clear from the scorch marks on the steel witness plate and the high-speed photography that there was significant combustion for the Al/PTFE projectiles vs. the 50.8-mm plates but not the 76.2-mm plates. The difference in combustion is either due to more of the Al/PTFE being consumed in the thicker target, the Al/PTFE being more pulverized in the thicker target, or the residual velocity of 600 – 700 m/s exiting the 76.2-mm targets being below the combustion threshold.

Pressure data was collected in all of the experiments but due to a variety of influences, the signals were noisy and the data not completely reliable. Ringing from the projectile impact could be seen as well as ringing from debris hitting the chamber sidewall and cables. (Debris impacts are also evident on the residual x-rays in Fig. 6.) While data quality was not sufficient for presentation, some valuable information could be distilled. For the 50.8-mm targets, peak transient pressures were on the order of 40 – 55 psi with sustained pressures of 15 – 20 psi. For the 76.2-mm targets, peak transient pressures were 20 – 23 psi with sustained pressures of 8 – 14 psi. For both target thicknesses, the Ni/Al casings delivered higher pressures. The pressure data is consistent with the increased combustion seen in the high-speed photography for the 50.8-mm targets. Finally, while the pressure data is informative in terms of relative combustion between the targets, in all cases, the pressures were below thresholds to damage material or incapacitate occupants.

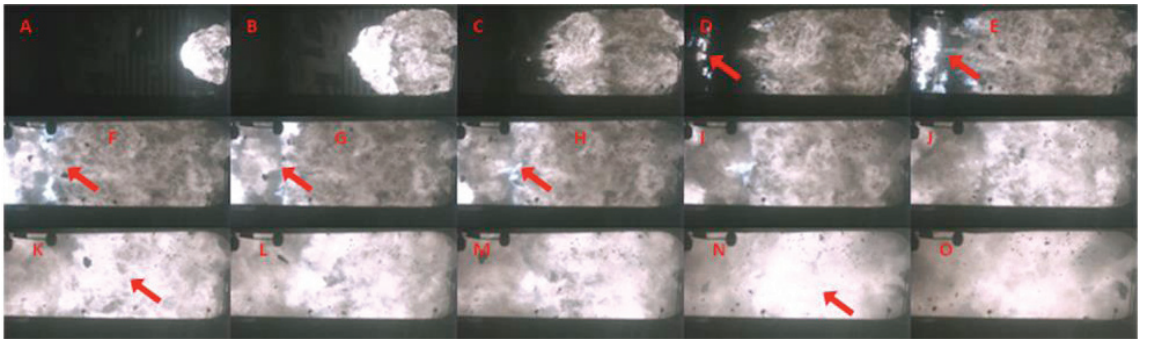

Fig. 8. Images of the fireball and debris exiting the 50.8-mm target for experiment #2500. Ignition of the Al/PTFE is significant and secondary combustion is evident.

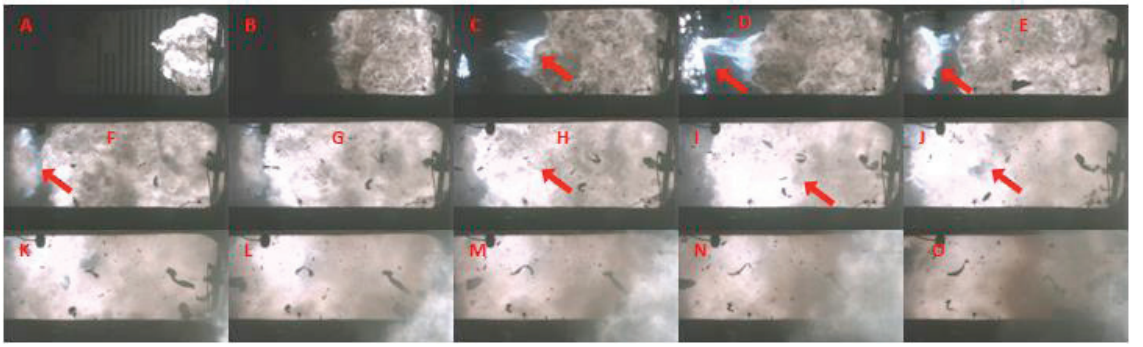

Fig. 9. Images of the fireball and debris exiting the 76.2-mm target for experiment #2504. Very little ignition of the Al/PTFE is seen and much less secondary combustion is seen.

4. Conclusions

This paper presented a series of experiments of nylon, aluminum, steel, and cased Al/PTFE projectiles striking aluminum armor at 2100 m/s to examine defeat mechanisms different than classical high-density penetrators. Projectile aspect ratios were very low and projectile diameters were similar to target thickness. The experiments demonstrated that depending on the level of ballistic over match, different fragment mass and spatial distributions could be obtained. The constant diameter, mass, and energy projectiles of aluminum and steel created nearly identical results with respect to debris character, however the steel projectile removed 10 – 25% more target mass for the two target thicknesses after normalizing by impact energy; indicating for the conditions examined, the steel projectile may be slightly preferable. However, it was clear that for the different levels of over match, the changes in the debris would have a dramatic affect on damage capacity behind the target. Of particular interest was whether the reactive material would change the character of the debris. Differences here are similar to the difference between aluminum and steel – debris characteristics are very similar, but on average, the AL/PTFE projectiles remove slightly less mass than the aluminum projectile. While the Al/PTFE projectiles did create a measurable pressure increase inside the impact chamber, the pressures were modest at best. However, video evidence certainly points to the noxious environment inside the impact chamber that is not present with the nylon, aluminum, and steel projectiles.

References

[1] Sorensen, B., Kimsey, K. and B., Love, "High-Velocity Impact of Low-Density Projectiles on Structural Aluminum Armor", IJIE, Vol 35, Issue 12, 2008.
[2] Ames, R., "Vented Chamber Calorimetry of Impact-Initiated Energetic Materials, 43rd AIAA Aerosapce Sciences Meeting and Exhibit, reno, Nevada, January, 2005.
[3] Ames, R., "Energy Release Characteristics of Impact-Initiated Energetic Materials", MRS Proceedings, Vol 896, 2005.
[4] Champagne, V., Helfritch, D., Leyman, P., Lempicki, R., and Grendahl, S., "The effects of gas and metal characterics on sprayed metal coatings", Journal of Modeling Simul. Mater. Sci. Eng, Vol 13, 2005.
[5] D.E. Grady and M.E. Kipp. Fragmentation properties of metals. *Int. J. Impact Engng* **20**, 293-308 (1997).